Int. J. Nano Dimens., 13 (3): 267-281, Summer 2022

ORIGINAL ARTICLE

Surface, structural and optical investigation on Poly Vinyl Alcohol (PVA)/Bi_2WO_6 nanocomposite films

Rashmi Saragur Nanjundaiah[1], Chandrashekar Hosur Kumara[1], Sangamesha Madanahalli Ankanathappa[2,*]

[1] Department of Industrial Production and Engineering, The National Institute of Engineering, Mysore-570 008, Karnataka, India

[2] Department of Chemistry, The National Institute of Engineering, Mysore- 570 008, Karnataka, India

Received 09 December 2021; revised 20 January 2022; accepted 09 February 2022; available online 22 February 2022

Abstract

Bismuth tungstate (Bi_2WO_6) emerged as one of the most capable chromogenic compounds among transition metal oxide having wide opto-electronic applications. It is an n-type semiconducting material having bandgap around ~2.7eV. Conversely, Nano Composite (NC) materials have been investigated in order to tailor the properties polymers and also to widen the applications. In this context Poly (vinyl alcohol)/ Bismuth tungstate (PVA/Bi_2WO_3) NC films were prepared with various weight ratio of Bi_2WO_6 content viz.0, 0.1, 0.2 0.4, and 0.8 wt%. The solution combustion method was employed to prepare Bi_2WO_6 nanoparticles (NPs). Subsequently, synergistic effect of polymer matrix and Bi_2WO_6 NPs is characterized and analysed to estimate the enhanced properties. The surface morphology of the NC's films was explored by Scanning Electron Microscopy (SEM). Elemental analysis is carried out using EDAX. The formation of polymer NC and its microstructural properties were investigated by X-ray diffraction technique and it is revealed that there is formation of orthorhombic phase for Bi_2WO_6 NPs with an average size of 35nm. Interaction of NP and PVA is studied using FT-IR spectrometer. The optical constants were evaluated by UV-visible spectrometer and it was found that NC films bandgap energy varied from 5.4 eV to 2.85eV for direct and from 4.57eV to 2.38eV for indirect bandgap. It is anticipated that these unique organic–inorganic NC materials are the emerging functional materials in the field of opto-electronics.

Keywords: *Bandgap; Bismuth Tungstate; Nanocomposite; Nanoparticles; PVA.*

How to cite this article

Saragur Nanjundaiah R., Hosur Kumara Ch., Madanahalli Ankanathappa S. Surface, structural and optical investigation on Poly Vinyl Alcohol (PVA)/Bi_2WO_6 nanocomposite films. Int. J. Nano Dimens., 2022; 13(3): 267-281.

INTRODUCTION

Aurivillius compounds with general formula $Bi_2A_{n-1}B_nO_{3n+3}$ (A = Ca, Sr, Ba, Pb, Na, K and B = Ti, Nb, Ta, Mo, W, Fe) are recognised to be main class of semiconductor metal oxides. These type of metal oxides has a distinctive layer of structure $(A_{n-1}B_nO_{3n+1})^{2-}$ is inserted between $(Bi_2O_2)^{2+}$ layers and have unique physicochemical properties. Bismuth tungstate (Bi_2WO_6) is a vital and simplest candidate among Aurivillius oxide family (n=1). This oxide has impressive properties like piezoelectricity, oxide anion conducting, pyroelectricity, non-rectilinear dielectric susceptibility, ferroelectricity and photocatalytic activity [1]. At room temperature, Bi_2WO_6 is orthorhombic with unit cell characteristics of a = 0.546 nm, b = 0.5436 nm, and c = 1.6427 nm [2]. Bi_2WO_6 is made up of accumulated layers of WO_6 octahedral sheets that share each corner Bi_2WO_6 [3]. Bi_2WO_6 is a photocatalytically active n-type semiconducting material with a bandgap of 2.7 eV, where an EC and EV band is nearly equal to 0.24 and 2.94 eV. [4]. Bi_2WO_6 consist of both valence and conduction

* Corresponding Author Email: *sangamesha.ma@gmail.com*

band, the domination in valence band occurs due to orbitals of O 2p and Bi 6s, in the case of conduction band domination is mainly due to the orbitals W 5d. The visible light sensitivity behaviour of Bi_2WO_6 material is due to the transition between the orbitals of conduction and valence band [5]. Bi_2WO_6, which has a layered perovskites structure, has been employed as an efficient photocatalyst for water splitting and photodegradation of organic molecules when exposed to visible light [6]. The photoactivity of the Bi_2WO_6 has shown to increase as a result of its unique layered structure, which accelerates electron transport to the surfaces [7] and also by altering its surface atomic structures [8]. Nanostructured bismuth tungstate has been discovered to have strong photocatalytic activity in the degradation process, owing to its unique ability in Organic Compound disintegration and advancement of O_2 when it's exposed to visible light [9]. It is also found that nanopowder synthesized using the molten salt method have a wider absorption edge and also have good light absorption characteristics not only within the ultraviolet but also in the visible light spectrum[10]. It also one of the visible-light active materials shows a lot of promise in terms of solar energy utilization [9].

In the recent years, nanoparticle-polymer NC's gained a lot of attraction since they exhibit unexpected properties [11, 12]. They are diverse from those of traditional materials due to the inclusion of nano-sized inorganic particles within the polymeric matrix and exhibits synergistic and hybrid properties [13]. Ease of manufacturing of organic polymers macromolecules combined with the improved mechanical and opto-electronic properties of nanoparticles have opens the fabrication novel devices [14]. Rajashekar *et al.* investigated PVA doped with ZnO and WO_3, revealed that adding ZnO and WO_3 at a weight percentage concentration of x=14% improves tensile strength and Young's modulus. Tensile strength is impacted by molecular weight due to the effect of entanglement [15].

Muhammad Bilal Tahir *et al.* has successfully synthesized Bi_2WO_6/PANI composites for the removal of ciprofloxacin (CIP) from wastewater and also achieved the production of hydrogen energy in the absence of sacrificial agents. The improved photocatalytic performance of Bi_2WO_6/PANI composite was mainly ascribed to the unique hierarchical structures, harvesting, higher surface area, and higher crystallinity. The current findings may provide new insights to fabricate nanomaterials for environmental and energy issues. Bi_2WO_6/PANI composite showed enhanced photocatalytic performance was mainly due to the exceptional hierarchical structures, prolonged absorption of visible light and crystallinity [16]. Cheng Cheng *et al.* fabricated Bismuth tungstate/ lotus fiber composite membrane (Bi_2WO_6/LF) and investigated visible-light photocatalytic activity for methylene blue. He reported that prepared Bi_2WO_6/LF shows excellent photocatalytic activity and degradation efficiency and it can be potentially applied in sewage disposal and environmental remediation [17].

In this view, our research work focussed on synthesis Bi_2WO_6 nanoparticles by an efficient and green method. The synthesis of Bi_2WO_6 is carried out by solution combustion method using naturally available lemon juice as a fuel. Additionally, PVA/ Bi_2WO_6 NC's is fabricated by doping Bi_2WO_6 nanoparticles with PVA polymer matrix by solution casting method to explore the optical properties of NC films. Nanocomposite films widened the applications to greater extant. Characterization of composite is attained to know the surface, structural and optical properties of the composite films. A cost-effective method for the synthesis of Bi_2WO_6 and PVA/Bi_2WO_6 composite films with controllable microstructure and optical property is achieved in the present research work.

EXPERIMENTAL WORK

Synthesis of Bi_2WO_6 Nanoparticles

All the chemicals used in this study are analytical grade and used without further purification. Synthesis of Bi_2WO_6 NP's is carried out solution combustion method. Solution Combustion Method (SCM) is a highly flexible process that permits the fruitful synthesis of a wide range of nano-sized ceramic materials. It is an exothermic redox reaction metal nitrate used as an oxidizing agent with a suitable fuel as a reducing agent. This method is highly cost effective for the synthesis of pure and homogeneous nanopowders. In SCM fuel play a major role in deciding the property of the prepared nanopowder.

$Bi(NO_3).5H_2O$ solution was prepared by using strong nitric acid with added 2.5 mL lemon juice as solution A. Then $Na_2WO_4.2H_2O$ solution was prepared by using 5 ml of distilled water with added 2.5 ml of lemon juice solution B [18].

Further, a homogeneous solution was prepared by mixing solution A and solution B and agitated. The resulted solution was preheated then placed in a muffle furnace at 400°C. A smouldering sort of combustion event occurs, and resulted in the formation of nanocrystalline Bismuth tungstate (Bi_2WO_6) powder, further the product is calcinated for 1 hour at 500°C. Overall chemical reactions in the formation of NP is as follows

$$2Bi(NO_3)_3 + Na_2WO_4 + 2H_2O \rightarrow Bi_2WO_6 + H_2O + 2NaOH + 2CO_2 + 3N_2$$

Urea and glycine are the most common fuels used for the synthesis of metal oxide nano powders with specific controlled stoichiometry. Nevertheless, number of researchers has published the use of complex fuels like citric acid, succinic acids, urea, monoethanolamine, alanine, and so on. Even though these fuels assist in the formation of nanosize particles, but additional calcination is essential to get high pure nanocrystalline powders. Recently, many researchers reported the synthesis of metal oxides nanoparticles using the natural plant materials like fruit juice, leaves extract, seeds, etc, and succeeded. In this present research work, we have used naturally available lemon juice as a fuel for the synthesis of Bi_2WO_6, since it simple, cost effective and environmental friendly in nature.

Fabrications of Polymer Nanocomposite Films (PVA/Bi_2WO_6)

Fabrication of PVA based polymer NC (PVA/Bi_2WO_6) films was done by using the solvent casting method. 7% PVA solution is used to prepare the NC's films and distilled water is used as solvent. At room temperature, to the aforesaid solution different weight percentages Bi_2WO_6 nanoparticles such as 0, 0.1, 0.2, 0.4, and 0.8 wt% were dispersed separately then poured to mold. The films were separated from the mold after drying completes and annealed at 80 ^{0}C for 1h. Schematic representation preparation of NC's film is as shown in Fig. 1.0.

Structural study of the pristine PVA, Bi_2WO_6 nanoparticle and PVA/Bi_2WO_6 NC's films were characterized by XRD (Bruker), with a wavelength of x-ray source λ=0.15406 nm and by FT-IR spectrometer. The surface study of the Fabricated NC's films is done by using Scanning Electron Microscopy. The optical absorption investigation has been carried out by UV Visible spectroscopy. The elemental analysis is carried out using EDAX.

RESULT AND DISCUSSION

Structural Study

A structural study of Bi_2WO_6, PVA, and NC's films with different nanoparticles concentrations (0, 0.1, 0.2, 0.4, and 0.8wt%) was carried out by using XRD. The XRD pattern of Bi_2WO_6 nanoparticles prepared by the SCM method followed calcinating at 500°C, show in Fig. 2. The as-synthesized Nanoparticles show diffraction peaks at 2θ= 27.77°, 32.66°, 43.33°, 49°, 52.18°, 57.22°, 60.07°, 64.22°, 67.37°, 74.29°, 78.49°, 80.97°, and 85.13°. The orthorhombic phase of Bi_2WO_6 is detected which are consistent with the literature survey [1, 13]. The high crystallinity of the samples is indicated by the strong and sharp

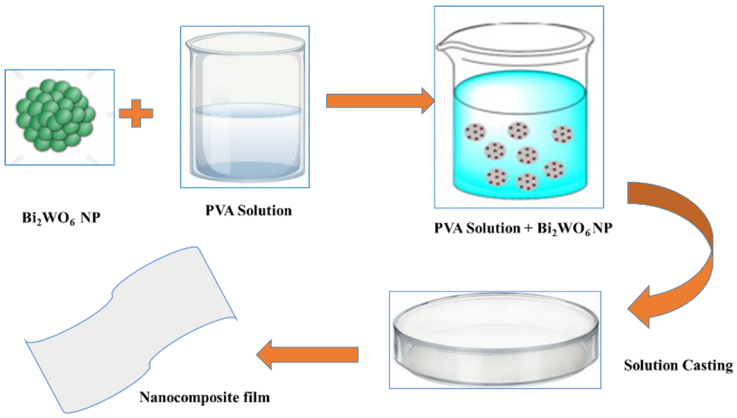

Fig. 1. Schematic representation of preparation of nanocomposite film.

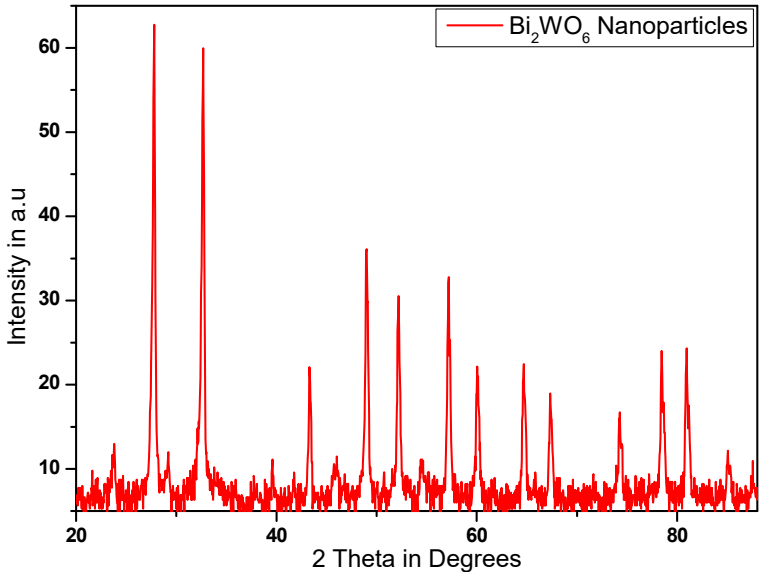

Fig. 2. XRD diffractograms of Bi_2WO_6 nanoparticles.

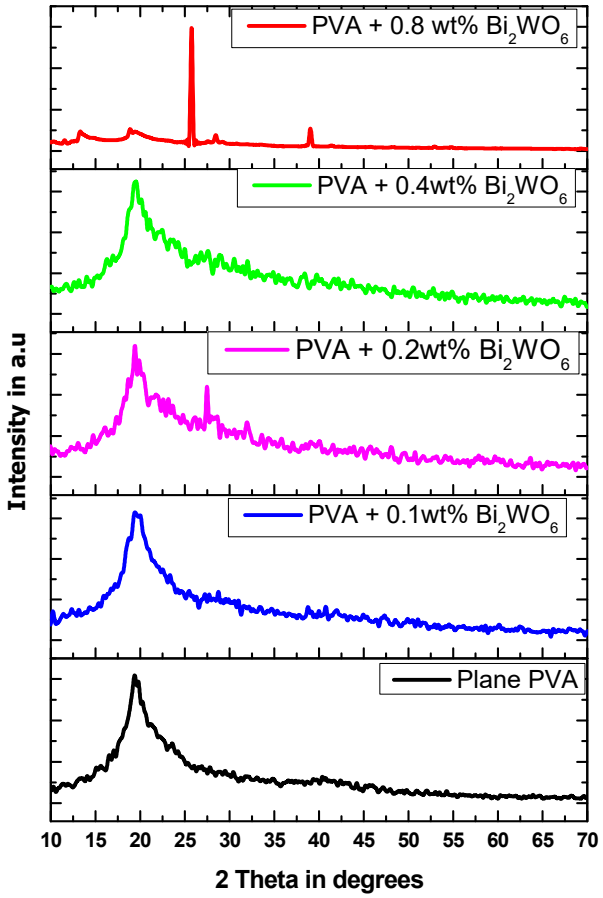

Fig. 3. XRD graph of PVA and PVA/Bi_2WO_6 nanocomposite films.

Table 1. Structural parameters of PVA/ Bi_2WO_6 films.

Composition of PVA/ Bi_2WO_6 (wt/wt%)	$2\theta_{max}$ (°)	FWHM (β)	d spacing (Å)	L (Å)	η	Lattice strain	R	SF
0/100	27.7702	0.22	0.184853	350.23	$8.15*10^{-6}$	0.0009	0.231	0.0008
100/0	19.4779	2.99	0.1303	26.13	0.001464	0.0129	0.163	0.0095
99.9/0.1	19.6664	2.85	0.13155	27.39	0.001332	0.0123	0.164	0.0091
99.8/0.2	19.5011	2.66	0.13046	29.32	0.001163	0.0115	0.163	0.0084
99.6/0.4	19.3499	2.99	0.12946	26.13	0.001464	0.0129	0.162	0.0094
99.2/0.8	18.8272	1.22	0.085	64.71	0.000239	0.0052	0.107	0.0031

peaks. The enhanced crystallization nature of Bi_2WO_6 NP sample, exhibits increased intensity and thinner diffraction peaks. There was no impurity peak found, which suggested that the as-synthesized Nanoparticles were highly pure. Fig. 3 shows the XRD pattern of pure PVA and NC films. Estimated microstructural parameters of PVA/ Bi_2WO_6 are detailed in Table 1.The Scherrer length (average particle size) of Pure Bi_2WO_6, PVA, and PVA/Bi_2WO_6 NC's have been calculated by the Scherrer formula.

$$L = \frac{k \times \lambda}{\beta \times cos\theta} \quad (1)$$

Where, k = 0.9, is a constant, as it relates to crystallite shape, λ is radiation wavelength θ is Bragg's angle, respectively: is FWHM of diffraction peak.

Fig. 3 depicts the XRD results of PVA/ Bi_2WO_6 NC's films in the range between 2θ= 10°-90°. The broad and intense diffraction band around, 2θ=19.4779° corresponding to the plane (101), illustrating the semi-crystalline nature of the pure PVA. This could be because of hydrogen bonding formation in the polymer chains of PVA, as well as intermolecular H- bonding within the polymer [19]. It's interesting to note that as the Bi_2WO_6 concentration in the PVA polymer matrix rises, the peak expands and the height lowers. This confirms that the PVA structure has transformed, as well as a decline in PVA crystalline phase. At 0.2wt% Bi_2WO_6, a new peak at 2θ=27.5483° appears, with significantly enhanced intensities due to the absorption of Bi_2WO_6 nanoparticles into the PVA. It is observed from the graph that there is a slight shift in the position of the peak in NC films. The shift indicates that there is an interaction between the PVA and nanoparticles in the composites.

It is observed from the XRD spectra of 0.8wt% PVA/Bi_2WO_6 NC, the intensity of the PVA peak is less, when compare to lower filler wt% NC films, it mainly because of the high filler wt% of Bi_2WO_6 nanoparticles, and increased strong intermolecular interaction between the polymer and NP within the polymer NC films. Subsequently, changes in the structural regularity of the main chains of the polymeric molecules also takes in the NC films, leads to the sharp diffraction peaks at high wt% composites film.

The Scherrer length (average particle size) of as prepared NP and for NC films is calculated using the relation L= 0.9λ/βcosΘ. It is found that average particle size increases steadily from pure up to 0.2 wt%, but then it is decreased for 0.4wt% again increased for 0.8 wt%. This apparent fluctuation in the particle size may be due to some aggregation of Bi_2WO_6 nanoparticles in the PVA polymer matrix [20, 21]. The variation in the FWHM value in the NC film with increase in Bi_2WO_6 content is due to a change or waning in the structure of PVA. From the XRD pattern it is observed that the diffraction peak of NC films grows wider and less intense as the number of nanoparticles wt% increases it is due to the mutual impact of PVA and Bi_2WO_6 at the interface. This change could be due to a decrease in the intermolecular H-bond interaction in between PVA as well as nanoparticles. This will have an impact on the matrix's free volume and also to cause the variations in the (d-spacing) is showed in table.1 [22]. In addition, for all PVA/ Bi_2WO_6 NC, the lattice strain ($\lambda \cos\theta/4$) and dislocation density (η= $1/L^2$) at the peak at 2θ = 19.9° have been determined and summarised in table.1. The resulted values for lattice strain decrease and dislocation density also decrease with an addition of Bi_2WO_6 Nanoparticle in the PVA polymer matrix. The degree of the recrystallization process in the polycrystalline films is primarily responsible for these variances. This means that doping alters the structural regularity of the polymeric molecule's major chains. Furthermore, the relation between inter-crystallite separation (R) and stacking fault

(SF), is as shown in the below formulas [21]:

$$R = \frac{5\times\lambda}{8\times sin\theta} \quad (2)$$

$$SF = \frac{2\pi^2}{45\times\sqrt{tan\theta}} \times \beta \quad (3)$$

Where λ= wavelength of X-ray, which is 1.5406 Å. θ is Diffraction angle in radians, and $\ddot{e}$ is FWHM in radians. It was noticed from Table 1 that, with decreasing SF Value there is a variation of R is indicated. In PVA/Bi_2WO_6 composite films, reduced R implies a rise in the number of PVA chains per unit of volume.

Nanoparticle and PVA interaction studies using FT-IR Spectrometer

The chemical interaction between Bi_2WO_6 nanoparticles and the functional groups of PVA polymer matrix can be substantiated with the FT-IR spectroscopic analysis of the prepared NC films. Fig. 4 displays the FT-IR spectra of the pure PVA and its Bi_2WO_6 nanoparticles doped NC film at 0.8wt% in the IR region. The FT-IR spectrum of pure PVA exhibits significant characteristic vibrations bands for presence the of O-H, C-H, C=C and C-O groups. The presence broad band witnessed between 3000 and 3600 cm^{-1} confirms the existence of hydroxyl (–OH) functional groups in PVA. Additional band at 2923cm^{-1} specifies asymmetric stretching mode of CH_2 group. The bands at 1356 and 1256cm^{-}

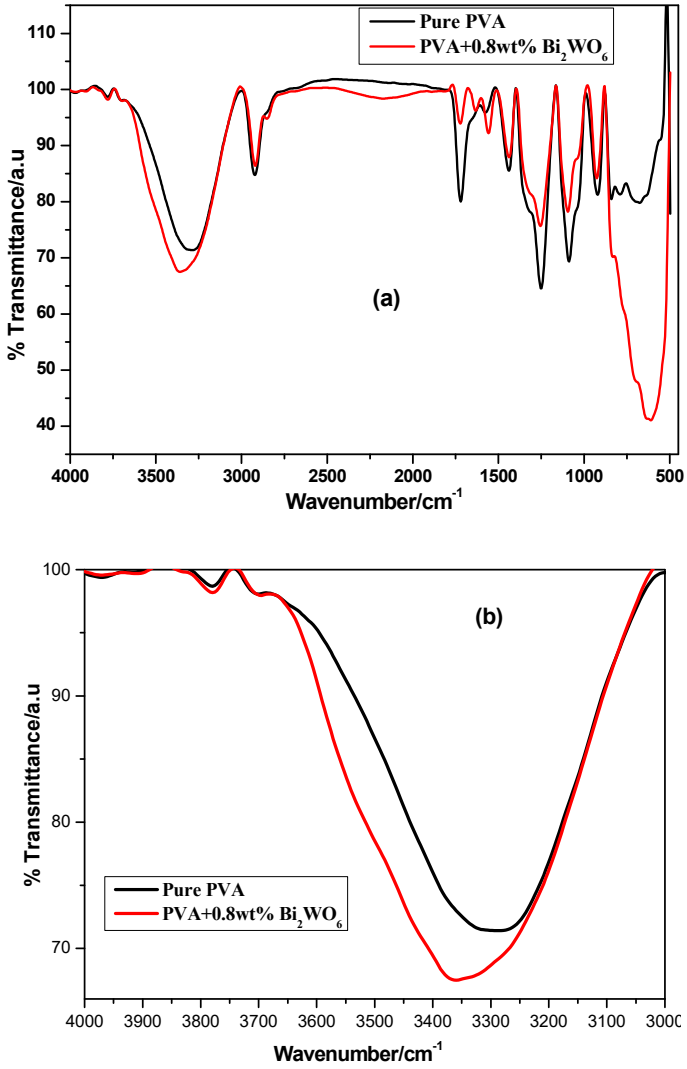

Fig. 4. (a) FT-IR spectra of pure PVA and 0.8wt% nanocomposite film, (b) FT-IR spectra of hydroxyl functional group region to show the effect of the NP on the –OH group of PVA.

[1] corresponds to vibrational motion of the C–H groups, where, the band at 851cm^{-1} rises due to the C–C stretching motion. The band detected at 1726 cm^{-1} for aliphatic acids or aldehydes and at 1095cm^{-1} for stretching mode of C–O bonds [23]. The FT-IR spectra of NC films shows intense bands confirm the insertion of nanoparticles also had major effect on the bonding interactions of PVA polymer matrix. The interaction among the metal oxide NP and the PVA polymer matrix may be due to hydrogen bonding (H-H) between the hydroxyl functional groups of PVA and the oxygen in Bi_2WO_6 nanoparticles. Fig. 4(b) shows the hydroxyl functional group (3000–3600cm^{-1}) region of the IR spectra. The alteration of the spectra from pure PVA polymer to the NC film is outward with the positions of hydroxyl group is crucial. Moreover, the positions band is slight shifted is due elongation of the hydroxyl bond payable to NP and polymer hydrogen bond formation [23, 24]. The data from the FT-IR spectrometer have good correlation with XRD results.

Surface Study

Surface properties of Bi_2WO_6 Nanoparticles, pure PVA, and PVA/Bi_2WO_6 composite films were revealed by using Scanning Electron Microscopy and shown Fig. 5. SEM was employed to study the morphological properties of the as-synthesized Bi_2WO_6 nanoparticles and the image is shown in

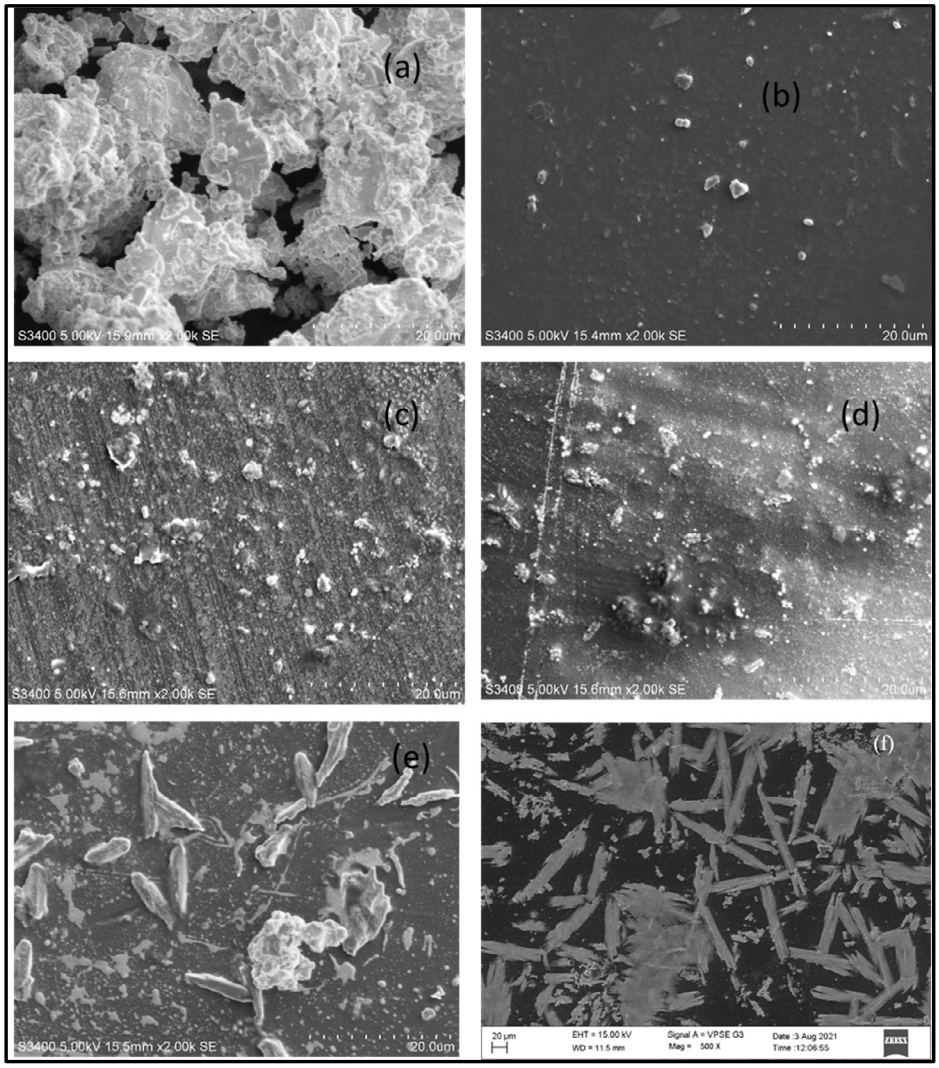

Fig. 5. SEM representation of (a) Bi_2WO_6 nanoparticles, (b) PVA+ 0wt% Bi_2WO_6 film, (c) PVA+ 0.1 wt% Bi_2WO_6 film, (d) PVA+ 0.2 wt% Bi_2WO_6 film, (e) PVA+ 0.4 wt% Bi_2WO_6 film, (f) PVA+ 0.8 wt% Bi_2WO_6 film.

Fig. 5(a). From the Fig. 5 (a), it is observed that the nanoparticles were piled together to form cluster like structures. Fig. 5(b) shows an SEM image of a pure PVA film with a smooth PVA matrix that has been uniformly prepared. The SEM representation of NC films (PVA/Bi_2WO_6) NC's films shown in Fig. 5 ((c)-(e)) show uniform and successful dispersion of Bi_2WO_6 Nanoparticles, where the density of NPs increased up to 0.4 wt% and it is noted that the average particle size in the films is around ~27nm in 0, 0.1, 0.2, and 0.4wt% PVA/Bi_2WO_6 films. Fig. 5(f) represents the SEM image of the PVA/Bi_2WO_6 of 0.8wt% NC films, observed that there is an agglomeration of nanoparticles in the film and also the average particle size is increased to ~138nm in the NC film this may due to increase in NP concentration. As the content of nanoparticles in the polymer NC's increases it is observed that particle size appears like needle like structure.

Elemental Analysis

Fig. 6 represents the EDX spectrum of PVA/Bi_2WO_6 NC's films of 0.8 wt% Bi_2WO_6 nanoparticles embedded in it. The composition of NC's films PVA/Bi_2WO_6 (0.8 wt%) and table 2 display the values that were obtained.

From table 2 it is noted that the existence of metals in the NC is Bi, and W, in the atomic ratio of 1:40 respectively. There is a presence of C in the NC that is from PVA. It is observed that Tungsten (W) is the major element (19.4 wt%) in the NC composition and bismuth is the minor element (0.5%) in the composition. The obtained value indicates the presence of Bi_2WO_6 nanoparticles in the NC's films.

Optical Study

Optical Absorption

Optical study of Pure PVA and PVA/Bi_2WO_6 films was carried out by UV-visible spectrometer. Fig. 7 displays the ultraviolet (UV)–visible spectroscopy absorption spectrum at a wavelength range of 200–1000 nm at room temperature for the pure PVA film and NC films (0, 0.1, 0.2, 0.4 and 0.8 wt%). It is observed from the spectrum that absorption of the polymer NC films increased as the Bi_2WO_6NPs concentration increases and the absorption edge gradually shifts towards the higher wavelength. The shifting of absorption edges could be due to Bi_2WO_6 aggregation in the polymeric matrix causing an increase in particle size [25]. The absorption peak of pure PVA film is at 280nm, it's due to the occurrence of a π–π^* electronic transition, which is a feature of

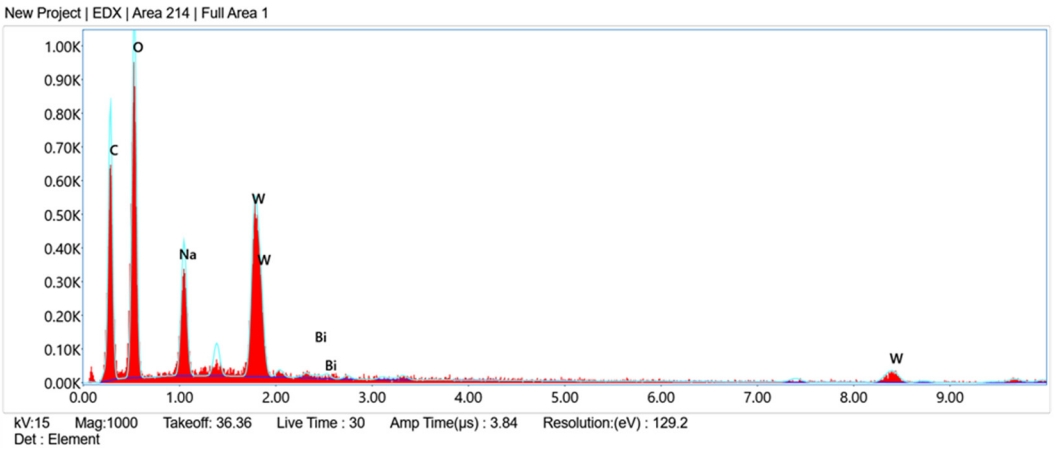

Fig. 6. Energy of dispersive X-ray (EDX) spectrum of PVA/Bi_2WO_6 (8 wt%) nanocomposite films.

Table 2. Elemental composition of PVA/Bi_2WO_6 (0.8 Wt%) nanocomposite films.

Element	Weight (%)	Atomic (%)	Error (%)
C K	34.4	50.4	11.2
O K	36.4	40.2	10.6
Na K	9.3	7.2	9.3
W M	19.4	1.9	6.9
Bi M	0.5	0.4	48.5

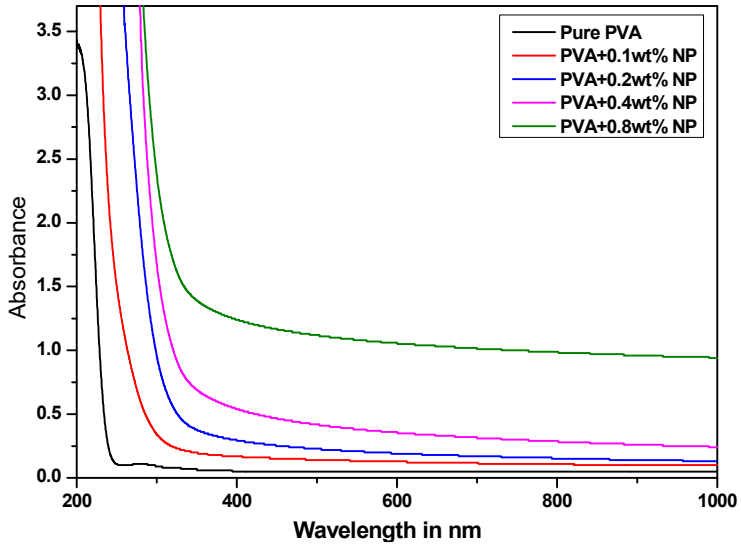

Fig. 7. Plots of absorbance V/S wavelength for PVA/ Bi_2WO_6 nanocomposite films.

conjugated (C=O) groups [26].

Absorption Coefficient

The absorption coefficient (α) is a significant parameter to tailer the dielectric properties of the material for particular application. The α was calculated using the following equation;

$$\boldsymbol{\alpha} = \frac{\mathbf{2.303 \times A}}{\boldsymbol{d}} \quad (4)$$

Where d is the thickness of the NC films, A is the Absorbance of NC. The absorption coefficient (α) as a function of photo energy (hν) for pure PVA and PVA/Bi_2WO_6 NC films, and the relation between $\boldsymbol{\alpha}$ and hν for pure PVA and its NC films, show in Fig. 8. It is observed from the graph that at low energies, the change in the absorption coefficient ($\boldsymbol{\alpha}$) is minimal, indicating that only a few electronic transitions are possible.

It is observed from the graph absorption coefficient ($\boldsymbol{\alpha}$) achieved in the case of composite films is less than 130 cm^{-1}, which due to and stipulates indirect electronic transition [25]. The Absorption edge energy of pure PVA film reduced from ~5.2 ev to ~2.2 eV at the 0.8 wt% of Bi_2WO_6introduction into the PVA matrix. Unexpectedly, as the Bi_2WO_6 wt% is increased, the absorption edge of the PVA/Bi_2WO_6 NC's films shifted to a lower hν value, as a result, lower in the bandgap value of NC films is originated due to interaction of NP with PVA. The increase in absorption coefficient ($\boldsymbol{\alpha}$) with increasing Bi_2WO_6 content is due to a change in the molecular structure of the PVA matrix [19]. This leads to electron transition in NPs and helps in forming conducting path in host polymer. This represents the prepared materials have lesser in energy gap which helps in absorption of the incident light. This property of the materials is suitable for the fabrication of opto-electronic devices. The decrease in the absorption edges with the increased NP content in the polymer matrix is related to high inter chain interactions with the polymer NC chains, resulting in denser conjugation stacking [19].

Optical Energy Bandgap

Using the Wood and Tauc relation, the optical energy bandgap (Eg) of NC's films is calculated based on UV absorption data [19].

$$(\boldsymbol{\alpha}\mathbf{h\nu}) \propto (\mathbf{h\nu}\text{-}\mathbf{E_g})^{\mathbf{n}} \quad (5)$$

$$(\boldsymbol{\alpha}\,\boldsymbol{\lambda}\,\mathbf{h\nu})^{\mathbf{1/n}} = \mathbf{B}\,\boldsymbol{\lambda}\,(\mathbf{h\nu}\text{-}\,\mathbf{E_g}) \quad (6)$$

Where B is related to constant Absorption value, $\boldsymbol{\alpha}$ is absorption coefficient, hν is the energy of the photon, E_g is the optical energy band gap and n is an index describing the electronic transaction's type.

The optical band gap (Eg) is a crucial metric for studying the interaction of the polymer matrix with

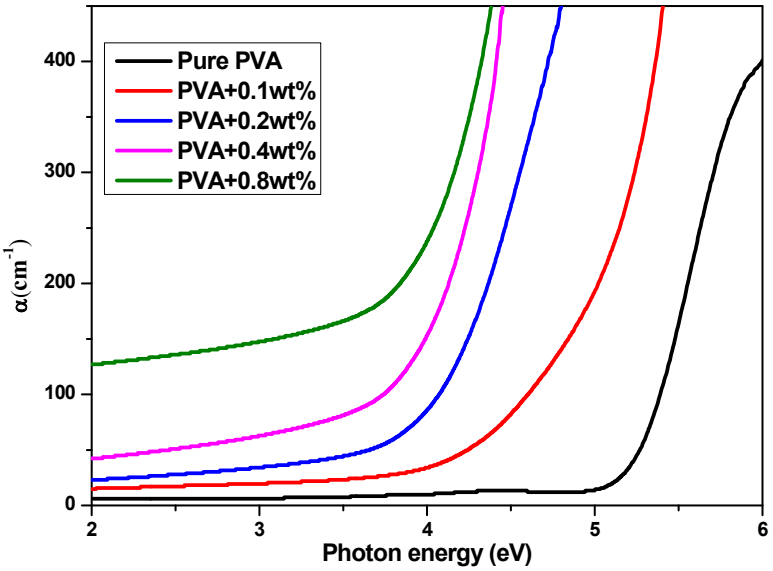

Fig. 8. α vs hν for PVA and its nanocomposites.

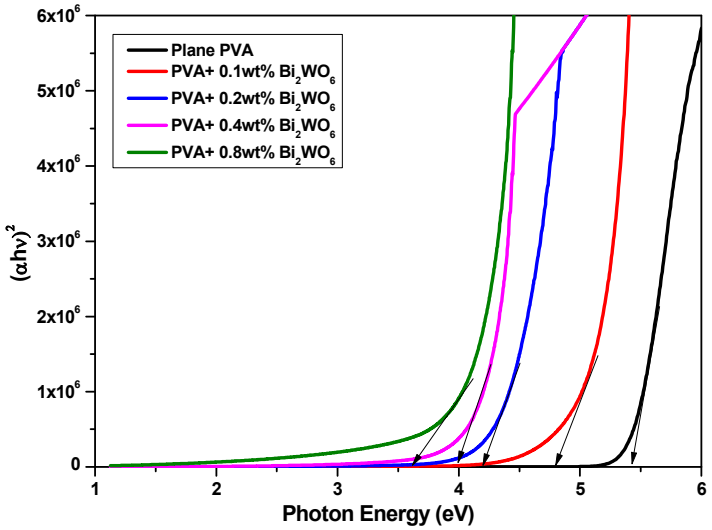

Fig. 9. $(\alpha h\nu)^2$ vs hν for a direct bandgap of PVA/Bi_2WO_6 nanocomposite films.

the NP in a polymer films. Plotting $(\alpha h\nu)^2$ vs hν, gives the relation for direct energy bandgap. Fig. 9, represents the direct bandgap of PVA/Bi_2WO_6 films (0wt%, 0.1wt%, 0.2wt%, 0.4wt% and 0.8wt%). From Fig.9, it's clear that shifting of Eg towards lower photon energy, as the nanoparticle content increases gradually from 0wt% to 0.8 wt% (~5.4eV to ~3.61 eV). Reduction in the band gap is because of the interaction of NP with the polymer matrix. The creation of defect states in the polymer matrix effectively reduces the value of the bandgap (Eg). When the value of n=2, the equation (6) results in the indirect bandgap of the PVA/ Bi_2WO_6 NC films. In indirect bandgap (Eg), was measured by plotting $(\alpha h\nu)^{1/2}$ vs hν for PVA/ Bi_2WO_6 NC's films. Table 3.0 summarizes the obtained band gap values of NC films

It was observed in Fig. 10, that absorption edge of PVA/Bi_2WO_6 NC's shift towards lower photon energy as the dopant's concentration increased gradually from 0 to 0.8 wt% (~4.57eV to ~2.38eV). The lowering in the bandgap might be due to the destruction of PVA and also the creation of localized states within the bandgap.

Table 3. Values of absorption edge and optical band gap of pure and its nanocomposites films.

PVA and its NC	absorption edge (eV)	Direct bandgap	Indirect bandgap
Pure PVA	5.24	5.41	4.76
PVA/Bi_2WO_6 NC 0.1wt%	4.61	4.79	3.57
PVA/Bi_2WO_6 NC 0.2wt%	3.90	4.21	3.21
PVA/Bi_2WO_6 NC 0.4wt%	3.69	3.98	3.05
PVA/Bi_2WO_6 NC 0.8wt%	3.31	3.61	2.68

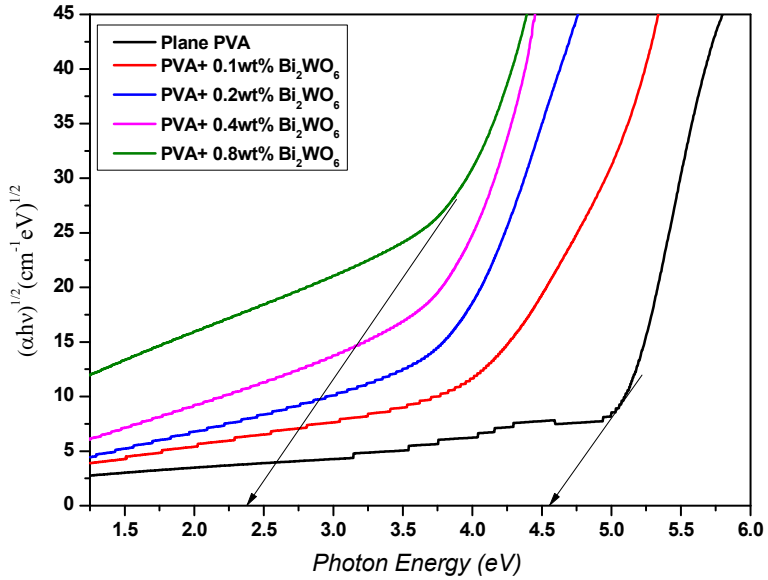

Fig. 10. $(\alpha h\nu)^{1/2}$ vs $h\nu$ for an indirect bandgap of PVA/Bi_2WO_6 nanocomposite films.

Refractive index and Extension Coefficient

The study of the refractive index (n) is performed because it is one of the critical parameters in deciding the appropriateness of a material for particular application [26]. The refractive index of PVA/Bi_2WO_6, NC films is calculated using following equation and calculated the refractive index (n) is displayed in Fig.11.

$$n = \frac{1+\sqrt{R}}{1-\sqrt{K}} \quad (7)$$

Fig. 11, indicates a significant increase of refractive index from 1.5 for PVA to 1.85 with increased wt% nanoparticles 0 to 0.4 wt% in PVA polymer matrix. This increase in *n* is attributed to the addition of Bi_2WO_6 in to the polymer that intern enhances the packing density [25] and also electronic polarizability. The marked increase in *n* values finds its application in optical areas like optoelectronic fabrication like anti-reflection coating, etc. The value of *n* for PVA/Bi_2WO_6 at 0.8 wt%, shows high because of increase in the density of the NC's films. These scatter of incident photons and cause the reflectance of the NC's films.

The imaginary portion of the complex refractive index is the extinction coefficient (*k*). The extinction coefficient of the NC films is calculated by using following equation

$$K = \frac{\alpha \times \lambda}{4 \times \pi} \quad (8)$$

Where *k* is a parameter that defines the amount of photonic energy lost in a unit surface area of NC's due to scattering and absorption.

Fig. 12, shows a variation of extinction coefficient (*k*) relating with wavelength for pure PVA and its Bi_2WO_6 NC's films. The energy of the photons in the UV region is sufficient to transfer electrons, due to this reason a small amount of energy is lost from the films which in turn decreases

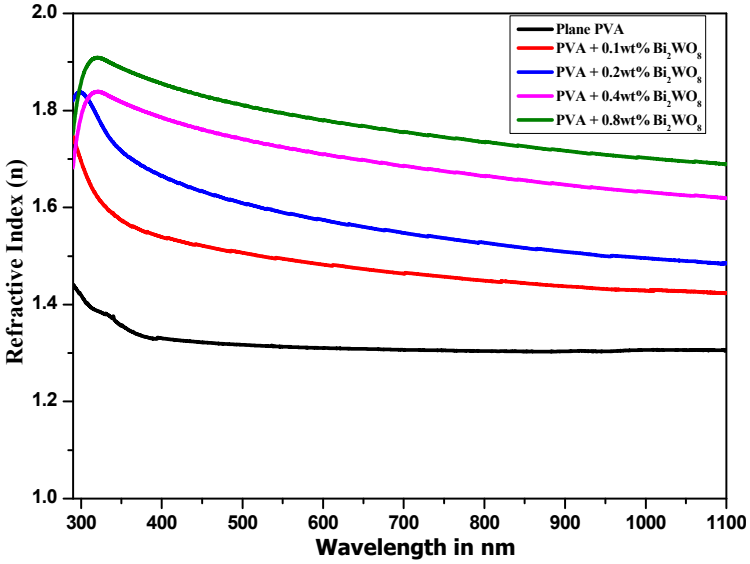

Fig. 11. Plot of refractive index vs wavelength of PVA and its nanocomposites.

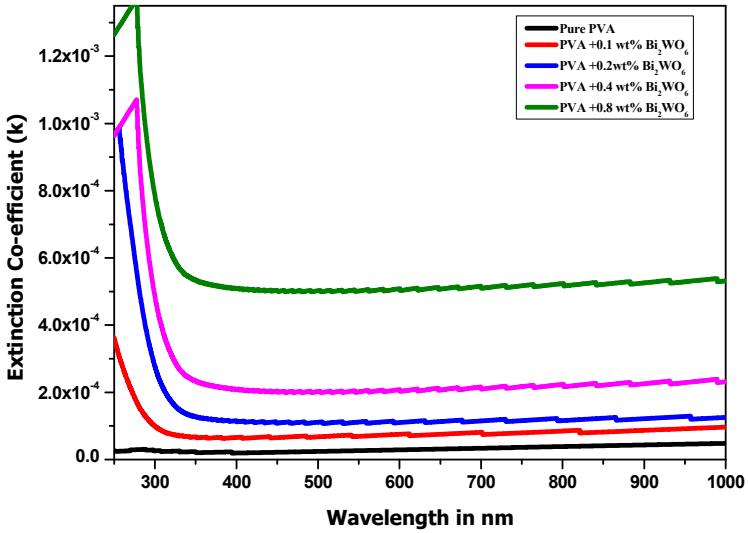

Fig. 12. Plot of extinction coefficient vs wavelength of PVA and its nanocomposites.

the extinction coefficient. Conversely, the energy of photons in the visible region is insufficient to achieve such a transfer as in the UV zone [27]. Furthermore, the k values increase when the Bi_2WO_6 content in the PVA polymer increases. This is because the absorption coefficient of polymeric films is rising i.e. (K is directly proportional to α).

Optical Dielectrics

The Optical dielectric properties have fundamental significance in tailoring the functioning of several opto-electronic devices. The real and imaginary parts of the dielectric constant of fabricated films are calculated using following equations.

$$\varepsilon_r = n^2 - K^2 \quad (9)$$

$$\varepsilon_i = 2 \times n \times K \quad (10)$$

Where ε_r and ε_i are the real and imaginary parts of dielectric constants. Fig. 13 shows the variations of the real dielectric part of PVA and its NC's as a function of wavelength. The Dielectric real portion is dependent on the refractive index of the material and the extinction coefficient value is

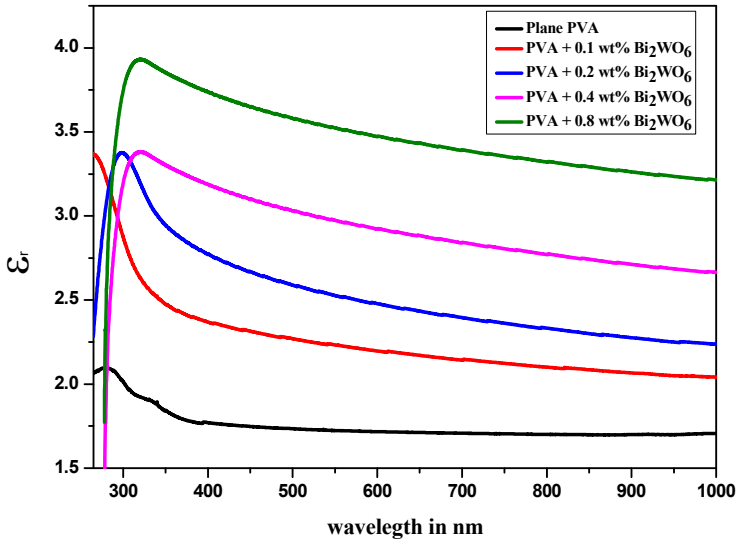

Fig. 13. Plot of real dielectric part vs wavelength for PVA/Bi_2WO_6.

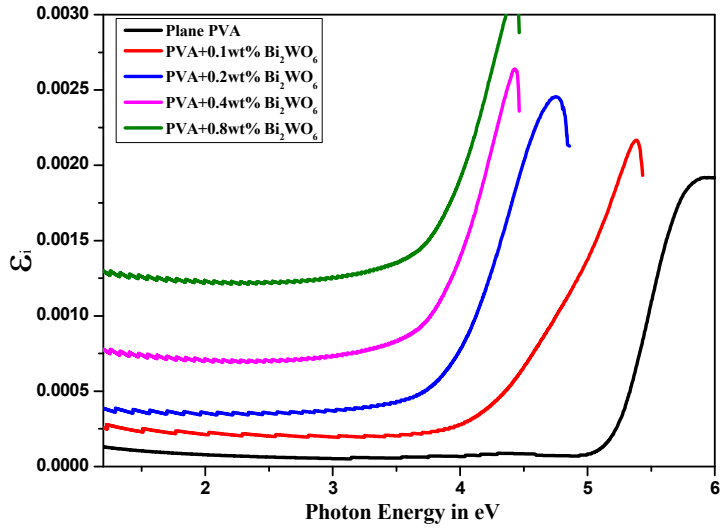

Fig.14. Plot of ε_i vs hν for PVA/Bi_2WO_6 nanocomposite films.

very small and maybe ignored as per the equation.

Fig. 13, shows it is evident that ε_r rises with increase in Bi_2WO_6 Nanoparticle content in the polymer matrix. Even after increasing wavelength that is beyond 350 nm, the real part of the dielectric constant for PVA/Bi_2WO_6 (0, 0.1, 0.2, and 0.4 wt%) NC films gradually decreases for a longer wavelength, and then it may become constant. This indicates that PVA/Bi_2WO_6 NC's have no response at longer wavelengths.

The absorption coefficient (α) is related to the imaginary dielectric constant (ε_i). Fig. 14 shows variations of the imaginary dielectric part *vs* photon energy (hν) of PVA/Bi_2WO_6 NC's films.

It is observed from the Fig. 14 that the imaginary part of PVA/Bi_2WO_6 NCe films moved from ~5.15 eV to ~2.15 eV as the concentration of Bi_2WO_6 Nanoparticles increases in the NC's films. These patterns could be understood that the reliance of the imaginary dielectric component (ε_i) on Extinction Coefficient (K) values, which becomes more significant.

The optical studies revealed that the band gap of the prepared PVA/Bi_2WO_6 NC's films is greatly reduced. It is reported elsewhere that the bandgap energy (Eg) of Bi_2WO_6 nanoparticles is

about 2.8 eV [28], but the NC film at higher filler wt% is achieved to 2.68eV (indirect). It is lesser than Bi_2WO_6 nanopowder also less than pure PVA. Doping of Bi_2WO_6 nanoparticles to PVA have significant effect in tuning the bandgap of PVA. This opens the wide applications in opto-electronics.

CONCLUSION

Bismuth tungstate (Bi_2WO_6) doped Poly Vinyl Alcohol (PVA) NC has been successfully fabricated by making use of solution casting method. The orthorhombic phase of the produced Bi_2WO_6 Nanoparticles was observed in XRD, with just an average size of 35 nm. The SEM imagining was indicative of a uniform distribution of Bi_2WO_6 nanoparticles over the surface and the distributed Bi_2WO_6 nanoparticles resembled a cluster consolidation. The bandgap values of NC's decrease from 5.41 eV to 3.61 eV for direct bandgap and from 4.76eV to 2.68 eV for indirect bandgap, as per the optical study. With an increase in the weight fraction of the Bi_2WO_6 nanoparticles from 0 to 8wt%, a noticeable enhancement in the refractive index of PVA/Bi_2WO_6 NC's films was witnessed, and the values corresponded to a range of 1.5 to 1.86. The Fabricated PVA/Bi_2WO_6 NC's had good optical properties with lesser bandgap value, may be employed in optoelectronic devices application.

ACKNOWLEDGEMENT

The author would like to express gratitude towards the Centre of Research and Development, The National Institute of Engineering, Mysuru for supporting, aid in experimental works and completion of the project.

CONFLICT OF INTEREST

There are no conflicts to declare.

REFERENCE

1. Wang B., Yang H., Xian T., Di L. J., Li R. S., Wang X. X., (2015), Synthesis of spherical Bi_2WO_6 nanoparticles by a hydrothermal route and their photocatalytic properties. *J. Nanomater.* 2015: Article ID 146327, 7 pages.
2. Somesh T. E., Shivakumar L. R., Sangamesha M. A., Demappa T., Siddaramaiah T., (2021), Polymer nanocomposites comprising PVA matrix and $AgGaO_2$ nanofillers: probing the effect of intercalation on optical and dielectric response for optoelectronic applications. *Ind. J. Sci. Technol.* 31: 2579-2589.
3. Sangamesha M. A.., Brunda M.., Vidyashree S.., Madhukar B. S.., (2021), Effect of In, Zr and Fe elements doped cerium oxide nanoprobes: Synthesis, characterization and their applications. *Materials Today: Proceed.* 46: 2400-2408.
4. Chunxiao Xu., Xiao R., Zhaohui W., Ying Xu., Gang Sh., Ge H., Gaorong H., (2009), Solvothermal preparation of Bi_2WO_6 nanocrystals with improved visible light photocatalytic activity. *Mater. Lett.* 63: 2194-2197.
5. Kumar Vijay B., Dambarudhar M., (2011), Formation of nanoscale tungsten oxide structures and colouration characteristics. *Bull. Mater. Sci.* 34: 435–442.
6. Cezarina C. M., Achim W. H., (2019), Review on the versatility of tungsten oxide coatings. *Phys. Status Solidi A*. 12: 1-16.
7. Liu X., Chen Ch., Chen Xi., Qian G., Wang J., Wang Ch., Zisheng L., (2018), WO_3 QDs enhanced photocatalytic and electrochemical perfomance of GO/TiO_2 composite. *Catalys. Today.* 315: 155–161.
8. Zhang X., Lu X., Shen Y., Han J., Yuan L., Gong L., Xu Z., Bai X., Wei M., Tong Y., (2011), Three-dimensional WO_3 nanostructures on carbon paper: Photoelectrochemical property and visible light driven photocatalysis. *Chem. Commun.* 20: 5804–5806.
9. Guo J., Li Y., Zhu S., Chen Z., Liu Q., Zhang D., Moon W. J., Song D. M., (2012), Synthesis of WO_3@Graphene composite for enhanced photocatalytic oxygen evolution from water. *RSC Adv.* 4: 1356–1363.
10. Vamvasakis I., Georgaki I., Vernardou D., Kenanakis G., Katsarakis N., (2015), Synthesis of WO_3 catalytic powders: Evaluation of photocatalytic activity under NUV/visible light irradiation and alkaline reaction pH. *J. Sol-Gel Sci. Technol.* 76: 120–128.
11. Sadeghi B., Jamali M., Kia Sh., Amini Nia A., Ghafari S., (2010), Synthesis and characterization of silver nanoparticles for antibacterial activity. *Int. J. Nano Dimens.* 1: 119-124.
12. Sadeghi B., Ghammamy Sh., Gholipour Z., Ghorchibeigy M., Amini Nia A., (2011), Gold/hydroxypropyl cellulose hybrid nanocomposite constructed with more complete coverage of gold nano-shell. *Micro & Nano Lett.* 4: 209–213.
13. Hariharan V., Radhakrishnan S., Parthibavarman M., Dhilipkumar R., Sekar C., (2011), Synthesis of polyethylene glycol (PEG) assisted tungsten oxide (WO_3) nanoparticles for l-dopa bio-sensing applications. *Talanta.* 85: 2166–2174.
14. Vamvasakis I., Georgaki I., Vernardou D., Kenanakis G., Katsarakis N., (2015), Synthesis of WO_3 catalytic powders: evaluation of photocatalytic activity under NUV/visible light irradiation and alkaline reaction pH. *J. Sol-Gel Sci. Technol.* 76: Corpus ID: 4839361.
15. Liu X., Jin A., Jia Y., Xia T., Deng C., Zhu M., Chen C., Chen X., (2017), Synergy of adsorption and visible-light photocatalytic degradation of methylene blue by a bifunctional Z-scheme heterojunction of WO_3/g-C_3N_4. *Appl. Surf. Sci.* 405: 359–371.
16. Muhammad Bilal T., Tasmia N., Ghulam N., Sagir M., Rafique M., Ahmed A., Muhammad Sh., (2020), Photocatalytic degradation and hydrogen evolution using bismuth tungstate based nanocomposites under visible light irradiation. *Int. J. Hydrog. Ene.* 45: 22833-22847.
17. Cheng Ch., Zoufei Du., Lin T., Jianwu L., Shouxiang J., Ronghui G., Ludan Z., (2018), Preparation and visible-light photocatalytic activity of bismuth tungstate/lotus fiber composite membrane. *Mater. Lett.* 210: 16-19.
18. Kodols M., Didrihsone S., Grabis J., (2014), Bi_2WO_6

nanoparticles prepared by combustion synthesis with different fuels and their photocatalytic activity. *In Key Eng. Mater.* 604: 93–101.
19. Laura M., Sanchez P., Shuttleworth S., Carolina W., Graciela Z., Vera A., Romina P., Ollier P., (2020), Physically-crosslinked polyvinyl alcohol composite hydrogels containing clays, carbonaceous materials and magnetic nanoparticles as fillers. *J. Environ. Chem. Eng.* 8: 103795-103801.
20. Sadeghi B., Pourahmad A., (2011), Synthesis of silver/poly(diallyldimethylammonium chloride) hybride nanocomposite. *Adv. Powder Technol.* 22: 669-673.
21. Parthibavarman M., Karthik M., Kumaresan A., Subramaniyan P., Venkatesan H., Poonguzhali R., Sathishkumar S., (2017), One-Step microwave synthesis of pure and Mn doped WO_3 nanoparticles and its structural, optical and electrochemical properties. *J. Mater. Sci. Mater. Electronics.* 28: 6635-6642.
22. Sanjeevamuthu S., Shanmugam V., Jeyaperumal K., Sundar V., (2020), Fabrication of PVA polymer films with improved antibacterial activity by fine-tuning via organic acids for food packaging applications. *Appl. Water Sci.* 10: 100-106.
23. Kumar Dey K., Kumar P., Ram Yadav R., Dhar A., Kumar Srivastava A., (2014), CuO nanoellipsoids for superior physicochemical response of biodegradable PVA. *RSC Adv.* 4: 10123-10129.
24. Siddaiaha T., Ojhaa P., Obularajugari Gopal N., Ramesh Kumara V., Ramu C.,, (2018), Structural, optical and thermal characterizations of PVA/MAA:EA polyblend films. *Mater. Res.* 21: e20170987.
25. Juliano Z., Ana B., Maira C., Maria G., Fabio Y., (2018), Polyvinyl alcohol (PVA) molecular weight and extrusion temperature in starch/PVA biodegradable sheets. *Polímeros.* 28: 256-265.
26. Tripathi S., Mehrotra G. K., Dutta P. K., (2009), Physicochemical and bioactivity of cross-linked chitosan–PVA film for food packaging applications. *Int. J. Biolog. Macromolec.* 4: 372-376.
27. Yao Y. R., Ma R., Song X. C., (2012), Hydrothermal synthesis of tungsten oxide nanoparticles. *Appl. Mechanic. Mater.* 268: 176–179.
28. Pramila S., Lakshmi Ranganatha V., Soundarya T. L., Ramu R., Nagaraju G., Mallikarjunaswamy C., (2021), Eco-mediated synthesis of visible active Bi_2WO_6 nanoparticles and its performance towards photocatalyst, supercapacitor, biosensor, and antioxidant activity. *J. Cluster Sci.* https://doi.org/10.1007/s10876-021-02147-9.